Sol-Gel Synthesis, Structural Characterization and Microwave Dielectric Properties of Bismuth Niobate Modified by Iron Inclusion

Susana Devesa, Manuel P.F. Graça and Luís C. Costa

Additional information is available at the end of the chapter

Abstract

The current progress in communication technologies is leading to extensive studies on the development of miniaturized electronic devices with high electromagnetic performances, reliability, and low cost. Contributing to this purpose, the development and study of new materials, with promising electric properties in radio and microwave ranges, have been subject of our research in particular niobate-based materials. Bismuth niobate, $BiNbO_4$, is a low-firing ceramic that has been studied for a variety of applications in the microelectronic industry. In this work, the microwave dielectric characterization of $(Bi_{1-x}Fe_x)NbO_4$ ($0.00 \leq x \leq 1.00$) samples, prepared by the sol-gel method and heat treated at specific temperatures, is performed and related with their structure and morphology. The structural data were obtained by X-ray diffraction and Raman spectroscopy and the morphology by scanning electron microscopy. The dielectric characterization in the microwave region was made using the small perturbation theory, with a resonant cavity operating in TE_{105} mode, at the frequency of 2.7 GHz. The results show that the sol-gel method has the advantage of allowing the formation of α-$BiNbO_4$ phase at lower temperatures when compared with conventional preparation methods, and that the inclusion of iron inhibits the formation of low- and high-temperature β-$BiNbO_4$ phases.

Keywords: bismuth niobate, sol-gel, X-ray diffraction, microwaves, dielectric properties

1. Introduction: state of the art

In the modern communication systems, where microwave frequencies are used, wireless equipment are indispensable [1]. Therefore, the development of smaller, faster, and multi-

functional equipment, with high electromagnetic performances and reliability, is an important technological challenge [2]. Since this goal can be achieved using ceramics technology, in the last decades a lot of research has been devoted to the improvement of dielectric ceramic materials that can be sintered at low temperature [3].

Bismuth oxides are recognized as low temperature-cofired ceramics (LTCC) and are considered promising materials for applications in the microelectronic industry [4]. In particular, bismuth niobate, $BiNbO_4$, has been studied to be used as resonators and filters in satellite and mobile communication systems [5].

The sintering temperatures of these microwave dielectrics cannot be high, since they need to cofire with low-loss conductors and low melting point electrodes, such as copper, silver, and gold [6]. Moreover, it is desirable that these ceramics have a high dielectric constant (ε'), a low dielectric loss (ε''), and a small coefficient of resonant frequency (τ_f) in the microwave range [7].

Bismuth niobate exists in two polymorph structures, an orthorhombic (α) phase (space group P_{nna}) and a triclinic (β) phase (space group P_1).

Figure 1 shows the crystal structures of (a) α-$BiNbO_4$ and (b) β-$BiNbO_4$. There are four formula units in the unit cell in both structures. The α structure consists of layers of vertex-sharing NbO_6 octahedra, which is normal to the c plane, with the Bi^{3+} positioned on the sites between these layers. The β phase presents pseudo layers of [Bi_2O_2] units connected with each other and surrounded by sheets of formula [NbO_4]n along the bc plane, in which the NbO_6 octahedra are joined at four vertices so that the two free oxygen atoms are in c axis. The Bi atoms hold these sheets together and are coordinated to eight oxygen atoms in the form of a much more distorted square antiprism. Summing up, the structure of α phase could be thought to be composed of two bismuth layers and two separated NbO_6 octahedral layers with different distortions. β-$BiNbO_4$ is composed of two bismuth layers and two joined octahedron layers [8, 9].
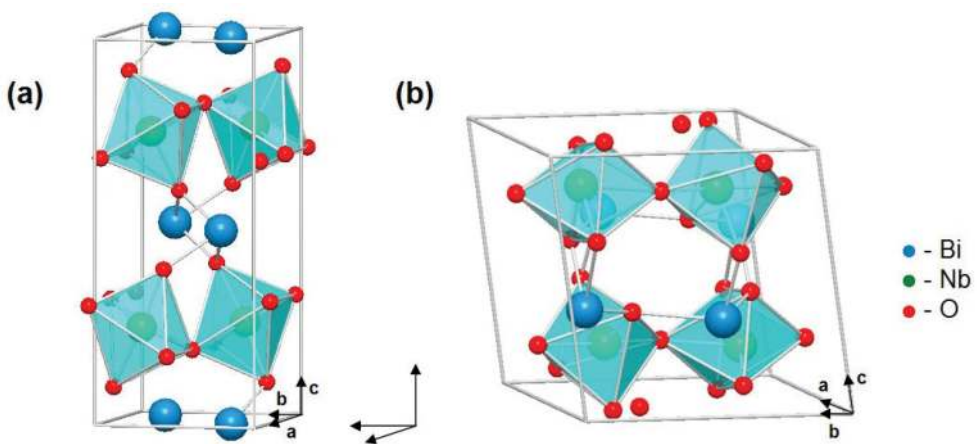

Figure 1. Schematic illustrations of crystal structures of (a) α-$BiNbO_4$ and (b) β-$BiNbO_4$.

According to previous studies, the transition of low temperature β-BiNbO$_4$ to α-BiNbO$_4$ occurs at temperatures between 600 and 750°C, with the opposite, and supposed irreversible, transition occurring at 1020/1050°C [10, 11]. In 2007, Zhou et al. [8] reported the transformation from high temperature β-BiNbO$_4$ to α-BiNbO$_4$ in bulk samples; however, this transition is still considered irreversible in powder samples.

BiNbO$_4$ ceramics can have low sintering temperature; however, they are difficult to densify without sintering aids [5]. The first attempt to improve the bismuth niobate properties was developed by Kagata et al. [12] in 1992. They used V$_2$O$_5$ and CuO as additives, with the purpose of densifying the ceramic materials without compromising their dielectric properties. Since then, in order to obtain higher densification, better dielectric properties, and reduce the sintering temperature, various attempts have been undertaken to improve the bismuth niobate properties as a microwave dielectric ceramic [4]. Besides the addition of different oxides, such as CuO [6], ZnO [13], V$_2$O$_5$ [14, 15], PbO, Bi$_2$O$_3$ [16], and Fe$_2$O$_3$ [17], several researchers tried to improve bismuth niobate properties through the substitution of bismuth for metals or lanthanides. In order to accomplish this task, (Bi$_{1-x}$R$_x$)NbO$_4$ compositions were developed and studied, where R represents different metals, such as Fe [18] or Pb [19], and different lanthanides, such as Ce, Nd, Dy, Er, La, Sm, Ta, Gd, and La [20–25].

The solid-state reaction has been the most common method to process bismuth niobate [1, 7, 8], which means its benefits and drawbacks are already documented in the literature. BiNbO$_4$ powders prepared by solid-state reaction result in high crystallinity, but not always in pure and homogeneous phases, because some metastable phases can be obtained under the same conditions [25]. This method may cause other problems such as large grain growth, segregation of components, and loss of stoichiometry due to the volatilization of bismuth at a high temperature [10].

The wet-chemical techniques, such as co-precipitation, alkoxide and citrate sol-gel methods, and flux method, were found to present several advantages: nanosize particles, high reactivity, very good homogeneity in composition, and lower energy consumption, because they operate in mild temperatures. However, in these methods, metastable phases can also be formed [1, 7, 10].

Co-precipitation is considered one of the most successful techniques for the synthesis of ultra-fine ceramic powders, having narrow particle size distribution. It is a less time-consuming method, since that can avoid complex steps such as refluxing of alkoxides. Nonetheless, an important drawback of co-precipitation is that all the cations should have similar solubility product [7, 10, 26].

The flux method is an alternative process that uses low-temperature liquid-phase reaction. According to previous studies, the BiNbO$_4$ prepared by the flux method exhibits higher crystallinity than that obtained by solid-state reaction; however, the successful application of this method depends on a large number of factors, like eutectic temperatures and solubility of solid components in the eutectic melts. Besides that, the decrease of the sintering temperature is not always achieved, since a proper combination of material/dopant is needed. In some cases, the mechanical separation between product and flux can be difficult [27, 28].

The sol-gel method, through citrate route, is considered a simple way to obtain stable precursors and stoichiometric fine powders which have been employed in the production of various oxides. This method is considered promising for achieving high homogeneity, since the formation of citrate complexes allows mixing the component cations in an atomic scale, thus they can immediately react with each other at relatively low temperatures [10, 13, 25].

In this work, the microwave dielectric properties of $(Bi_{1-x}Fe_x)NbO_4$ ($0.00 \leq x \leq 1.00$) samples, prepared by sol-gel method, through the citrate route, and heat-treated at specific temperatures, are studied. Since it is recognized that the behavior of functional materials is intrinsically linked to their structures [29], a structural characterization of the obtained samples was performed, using X-ray diffraction (XRD). Furthermore, to verify the structure consistency between low- and high-temperature β-$BiNbO_4$, and to better understand the phase transition process, the Raman spectroscopy was performed [10].

Since it is recognized that the dielectric properties can be related with density, porosity, and grain boundaries [20], the density of the samples was measured, using Archimedes method, and the morphology data was obtained by scanning electron microscopy (SEM).

2. Case study

2.1. Samples preparation

$(Bi_{1-x}Fe_x)NbO_4$ powders were prepared by the sol-gel method. Bismuth nitrate ($Bi(NO_3)_3 \cdot 5H_2O$), niobium chloride ($NbCl_5$), iron nitrate ($Fe(NO_3) \cdot 9H_2O$), were used as starting materials and citric acid and ethylene glycol as chelating agent and reaction medium, respectively. All reagents used in the whole procedure were of analytical grade. The starting materials, with purities >99.9%, were supplied by Mateck and Merk and the chelating agent and reaction medium by Sigma-Aldrich. Bismuth nitrate, niobium chloride, and iron nitrate solutions were prepared in minor amounts of hydrogen peroxide (3%, V/V), combined in the corresponding molar ratio, and then added to citric acid and ethylene glycol. The obtained mixtures were stirred, to promote the solubility, until clear colloidal suspensions were obtained.

The obtained solutions were dried to evaporate the solvent: the solution of the reference sample, $x = 0.00$, was dried at 400°C, for 48 h; the solutions with $0.25 < x < 0.75$ were dried at 300°C, for 60 h; the solution with $x = 1.0$ was dried at 300°C, for 24 h. Subsequently, the obtained powders were thermally analyzed by differential thermal analysis (DTA), performed in a Linseis Apparatus type L92/095, in the temperature range of 20–1200°C, with a heating rate of 5 and 10°C/min, using Al_2O_3 as reference. Finally, the dry powders were pressed into cylinders and heat-treated, according to the DTA results, at temperatures between 500 and 1200°C, using a dwell time of 4 h, with a heating rate of 5°C/min.

2.2. Experimental methods

The structural characterization was performed using X-ray diffraction (XRD). The patterns data was obtained on a X'Pert MPD Philips diffractometer and on an Empyrean diffractometer (CuK α radiation, $\lambda = 1.54060$ Å) at 45 kV and 40 mA, in a Bragg–Brentano parafocusing

optics configuration. The step counting method was used, with a step of 0.02° and a time per step of 1 s, with a 2θ angle range of 10–60°.

Raman spectroscopy measurements were performed at room temperature, in backscattering geometry, with a 441.6 nm laser line using a HR-800-UV Jobin Yvon Horiba spectrometer. A microscope objective focused the exciting light onto the sample.

The ceramics bulk density was measured using the Archimedes method in reference to water.

The morphology of the sintered samples was analyzed by scanning electron microscopy (SEM), using a TESCAN-Vega III. The samples were covered with carbon before microscopic observation.

The measurement of the complex permittivity was made using the small perturbation theory, with a cavity operating in TE_{105} mode, at resonant frequency of 2.7 GHz. These measurements were made using a HP 8753D coupled to the cavity resonator.

Microwave resonant cavities have been used for evaluating the dielectric properties of geo-metrically defined samples, when the cavity is calibrated with dimensionally identical sample of known permittivity.

For a given cavity and a sample of regular shape and well-defined dimensions, it is pos-sible to determine the permittivity of the material. The permittivity values of a sample can be obtained through the changes in the resonant frequency, Δf, and in the inverse of the quality factor $\Delta (1/Q)$ of the resonant cavity, when introducing a sample in the cavity, where the elec-tric field is maximal [30–33].

The shift in the resonant frequency of the cavity, Δf, can be related to the real part of the complex permittivity, ε', whereas the change in the inverse of the quality factor of the cavity, $\Delta (1/Q)$, can be related with the imaginary part, ε''.

Considering only the first-order perturbation in the electric field caused by the sample [30–33], we obtain

$$\varepsilon' = K \frac{\Delta f}{f_0} \frac{V}{v} + 1 \tag{1}$$

$$\varepsilon'' = \frac{K}{2} \Delta \left(\frac{1}{Q} \right) \frac{V}{v} \tag{2}$$

where K is a constant related to the depolarization factor, which depends upon the geometric parameters, v and V are the volumes of the sample and the cavity, respectively, and f_0 is the resonance frequency of the cavity. Using a sample of known permittivity, in our case polytet-rafluorethylene (PTFE), we can determine the constant K.

2.3. Results and discussion

2.3.1. DTA

The DTA data of the powders with $x = 0.00$ ($BiNbO_4$) and $x = 1.00$ ($FeNbO_4$) are shown in **Figure 2**. In **Figure 2(a)**, one can see the occurrence of three exothermic peaks, at 649, 1043,
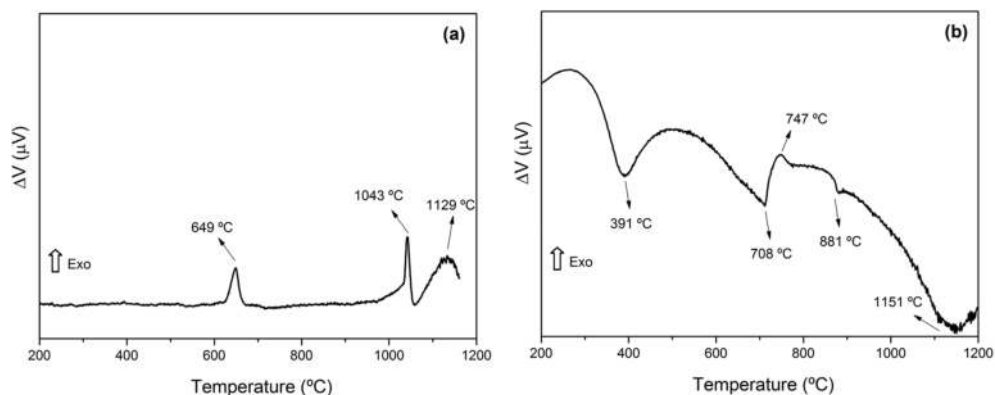
Figure 2. (a) DTA of BiNbO$_4$ powder, $x = 0.00$, heated at the rate of 10°C/min; (b) DTA of FeNbO$_4$ powder, $x = 1.00$, heated at the rate of 5°C/min.

and 1129°C. **Figure 2(b)** shows four endothermic phenomena at 391, 708, 881, and 1151°C. The peak that occurs at 391°C is due to the decomposition of residual organic compounds that were not released during the drying process.

The powders with $0.25 \leq x \leq 0.75$ were also thermally analyzed. When $x = 0.25$, three exothermic phenomena were identified, centered at 519, 637, and 1054°C. With $x = 0.50$, we can highlight once again three exothermic peaks, at 489, 556, and 637°C. The powder with $x = 0.75$ shows two exothermic peaks at 485 and 1157°C.

The heat treatments were made in agreement with these results, as shown in **Table 1**.

x	Treatment temperatures (°C)								
	500	650	800	850	1000	1050	1100	1150	1200
0.00	×	×	−	×	−	×	−	×	a
0.25	×	×	×	−	−	−	×	−	−
0.50	×	×	×	−	−	−	×	−	−
0.75	×	×	×	−	−	−	×	−	−
1.00	×	×	−	×	×	−	−	−	×

[a]The heat treatment performed at 1200°C promoted the fusion of the powders.

Table 1. Heat treatments performed in the cylindrical samples.

2.3.2. XRD pattern analysis

Figure 3 shows the X-ray diffraction patterns of $(Bi_{1-x}Fe_x)NbO_4$ powders, for $x = 0.00$, **Figure 3(a)**, and $x = 1.00$, **Figure 3(b)**.

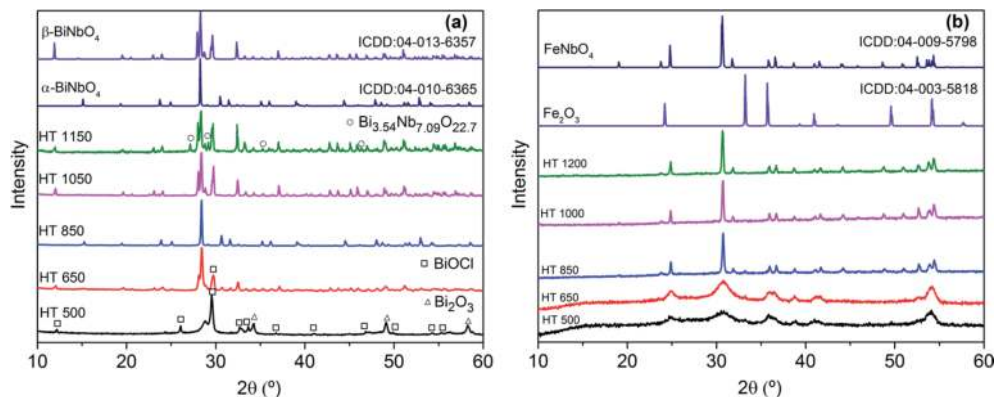**Figure 3.** X-ray diffraction patterns of $(Bi_{1-x}Fe_x)NbO_4$ samples for (a) $x = 0.00$ and (b) $x = 1.00$.

Analyzing the diffraction patterns shown in **Figure 3(a)**, for the powders treated at 500°C, there are two secondary phases Bi_2O_3 and BiOCl, and the beginning of the β and α phases formation. The sample treated at 650°C is a combination of α- and β-$BiNbO_4$ phases, with the secondary phase BiOCl still present. After the treatment of the samples at 850°C, the X-ray diffraction pattern shows the formation of pure orthorhombic $BiNbO_4$ and, with a further temperature increase, this phase is converted to triclinic $BiNbO_4$. For the highest treatment temperature, the volatile nature of Bi^{3+} ions, at elevated temperatures, promotes the formation of a non-stoichiometric phase of bismuth niobate, $Bi_{3.54}Nb_{7.09}O_{22.7}$.

Therefore, the DTA exothermic band centered at 649°C can be due to the formation of α-$BiNbO_4$, and the exothermic reaction occurring at 1043°C can be attributed to the conversion of α-$BiNbO_4$ to β-$BiNbO_4$. The thermal treatment at 1200°C promoted the fusion of the samples; consequently, there is no exact information about the exothermic phenomenon at 1181°C. However, the formation of a non-stoichiometric phase, due to the volatile nature of bismuth [3], is predictable.

In **Figure 3(b)**, it is observed the formation of monoclinic $FeNbO_4$, even at the lowest heat-treatment temperature. For the treatment temperatures from 500 to 1000°C, one additional phase was detected, Fe_2O_3, with a content equal or inferior at 5%. For the 1200°C heat treatment, single-phase $FeNbO_4$ sample was obtained. Therefore, the DTA exothermic phenomena appearing at 747°C can be related with an improvement of the crystallization process of $FeNbO_4$ and the phenomena visible at 1151°C can be attributed to the decomposition of the Fe_2O_3, and consequent formation of $FeNbO_4$, with the niobium still present in the amorphous form. The increase of the amplitude and decrease of the half-width of the obtained XRD peaks, and of the Raman bands, shows that the increase of the heat treatment temperature promotes an increase of the crystallinity.

The samples with $0.25 \leq x \leq 0.75$ were also characterized using X-ray diffraction, with the diffraction patterns shown in **Figure 4** and the present phases identified in **Table 2**. Besides the
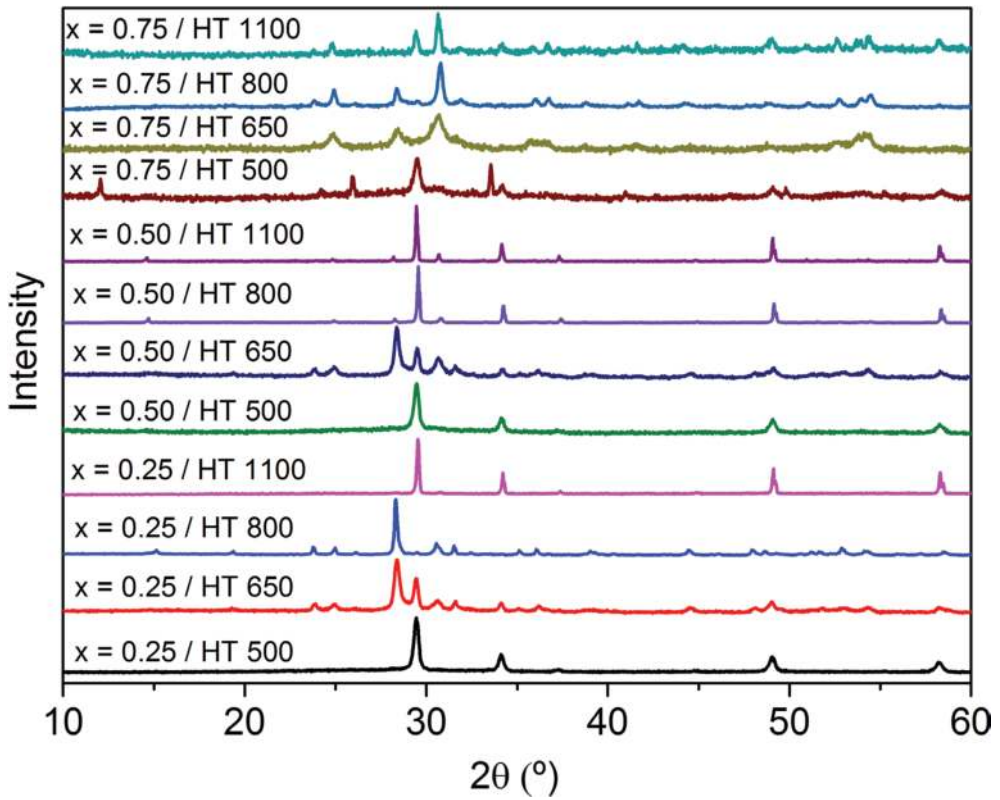
Figure 4. X-ray diffraction patterns of $(Bi_{1-x}Fe_x)NbO_4$ samples for $0.25 \leq x \leq 0.75$.

	HT 500	HT 650	HT 800	HT 1100
$x = 0.25$	$Bi_{1.34}Fe_{0.66}Nb_{1.34}O_{6.35}$	α-$BiNbO_4$ $Bi_{1.34}Fe_{0.66}Nb_{1.34}O_{6.35}$	α-$BiNbO_4$ $FeNbO_4$ Bi_2O_3	$Bi_{1.721}Fe_{1.056}Nb_{1.134}O_7$ $BiFeO_3$
$x = 0.50$	$Bi_{1.34}Fe_{0.66}Nb_{1.34}O_{6.35}$	α-$BiNbO_4$ $Bi_{1.34}Fe_{0.66}Nb_{1.34}O_{6.35}$	$Bi_{1.721}Fe_{1.056}Nb_{1.134}O_7$ $FeNbO_4$	$Bi_{1.721}Fe_{1.056}Nb_{1.134}O_7$ $FeNbO_4$
$x = 0.75$	$Bi_{15}NbO_{25}$ Fe_2O_3 $Fe_{0.33}Nb_{0.67}O_2$	$FeNbO_4$ Bi_2O_3	$FeNbO_4$ Bi_2O_3	$FeNbO_4$ $Bi_{15}NbO_{25}$

Table 2. Identification of the crystalline phases of $(Bi_{1-x}Fe_x)NbO_4$ samples for $0.25 \leq x \leq 0.75$.

expected phases like α-$BiNbO_4$ and $FeNbO_4$, there was the formation of two non-stoichiometric phases, $Bi_{1.34}Fe_{0.66}Nb_{1.34}O_{6.35}$ and $Bi_{1.721}Fe_{1.056}Nb_{1.134}O_7$, where the substitution of Bi^{3+} for Fe^{3+} ions was successful, and five more secondary phases. The absence of β-$BiNbO_4$ in the samples treated at 1100°C was unexpected, since the transition of α- to β-$BiNbO_4$ occurs, according to previous works, at 1020/1050°C [10, 11], and happened in the host sample at 1043°C.

Confronting the X-ray diffraction data with the DTA, it is possible to assume that for the samples with $x = 0.25$ and 0.50, the exothermic peaks can be related with the formation of the $Bi_{1.34}Fe_{0.66}Nb_{1.34}O_{6.35}$, α-BiNbO$_4$, and $Bi_{1.721}Fe_{1.056}Nb_{1.134}O_7$ phases, respectively. Since these three peaks are dislocated for lower temperatures in the sample with $x = 0.50$, it means that the energy required for these phase transformations decreases with the increase of the amount of iron. Considering the sample with $x = 0.75$, the peak occurring at 485°C can be assigned to the formation of $Bi_{15}NbO_{25}$ and the one centered at 1157°C should be related to a non-stoichiometric phase formation.

In the present study, one can conclude that the sol-gel method has the advantage of forming the orthorhombic BiNbO$_4$ phase at even lower temperatures, since the sample with $x = 0.00$, treated at 500°C, presents already the α phase, and that the inclusion of iron inhibits the formation of low- and high-temperature triclinic bismuth niobate.

2.3.3. Raman spectroscopy analysis

The Raman spectroscopy data of $(Bi_{1-x}Fe_x)NbO_4$ powders, for $x = 0.00$ and $x = 1.00$, are presented in **Figure 5**.

In **Figure 5(a)**, we can see that the Raman spectrum of the sample treated at 850°C, pure orthorhombic BiNbO$_4$, is less complex than the spectra were the triclinic BiNbO$_4$ is present. This result was expected since the lowered symmetry of the triclinic phase produces more Raman active modes [10]. The samples treated at 500, 650, 1050, and 1150°C possess peaks at 102, 450, and 687 cm^{-1} attributed to the vibration modes of β-BiNbO$_4$. This means that both low and high temperature β-BiNbO$_4$ have identical vibration modes. In the sample treated at 850°C, where only α-BiNbO$_4$ was detected, these peaks are absent. Furthermore, the peaks at 139 and 199 cm^{-1} are distinctive of the orthorhombic BiNbO$_4$, which explains their absence in the spectra of the samples treated at 1050 and 1150°C. All the peaks present in these two samples are attributed to triclinic BiNbO$_4$ [10, 34]. No vibration that can be assigned to non-stoichiometric phase $Bi_{3.54}Nb_{7.09}O_{22.7}$ was detected.
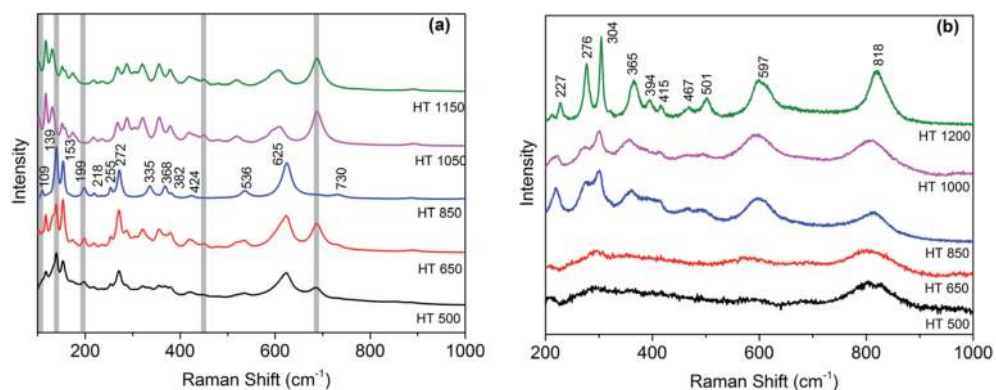

Figure 5. Raman spectra of $(Bi_{1-x}Fe_x)NbO_4$ samples for (a) $x = 0.00$ and (b) $x = 1.00$.

In the spectra presented in **Figure 5(b)**, all the detected bands are attributed vibrations of the base units of the monoclinic $FeNbO_4$ phase. The Nb—O stretching bands were observed at 276, 394, 597, and 818 cm^{-1}, and the bands visible at 365 and 467 cm^{-1} are exclusively for the monoclinic $FeNbO_4$ [35–38]. With the increase of the temperature, it can be seen a better definition of bands, which is consistent with the increase of the crystallinity of the samples.

The Raman spectroscopy data of $(Bi_{1-x}Fe_x)NbO_4$ powders, with $0.25 \leq x \leq 0.75$, are presented in **Figure 6**. Regardless of the x value, the obtained data shows that the crystallinity increases with the temperature.
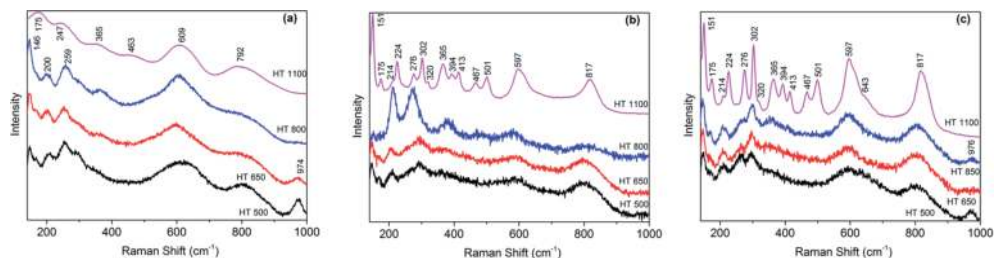

Figure 6. Raman spectra of $(Bi_{1-x}Fe_x)NbO_4$ samples for (a) $x = 0.25$, (b) $x = 0.50$, and (c) $x = 0.75$.

In the samples with $x = 0.25$ treated at 650 and 850°C and $x = 0.50$ treated at 650°C, the peak occurring at 200 cm^{-1} is distinctive of the orthorhombic $BiNbO_4$. On the other hand, the peaks visible at 224, 276, 304, 365, 394, 467, 501, 597, and 817 can be assigned to $FeNbO_4$.

2.3.4. Density

The bulk density values of $(Bi_{1-x}Fe_x)NbO_4$ ceramics, for $x = 0.00$ and $x = 1.00$, in reference to water versus treatment temperature are shown in **Figure 7**.

The bulk density increase with the treatment temperature increase is clearly visible for both the series of samples, and it allows to predict that porosity decreases at higher treatment temperatures.

The theoretical density of β-$BiNbO_4$ ceramic (7.5 g/cm^3) is higher than that of α-$BiNbO_4$ ceramic (7.345 g/cm^3) [21, 22]. Thus, and considering the samples with $x = 0.00$, the increase of bulk density of $BiNbO_4$ ceramics from 850 to 1050°C can be due to the orthorhombic-triclinic phase transformation of $BiNbO_4$. According to the literature, it is very difficult to densify the ceramics above 85% of theoretical density without sintering additives [24]. However, in the sample treated at 1150°C, the density is 85.3% of the theoretical density and that was slightly above the pointed level.

Considering now the samples with $x = 1.00$, and knowing that the theoretical density of $FeNbO_4$ ceramic is 5.40 g/cm^3 [39], we can determine that for the highest heat treatment, the only one where pure $FeNbO_4$ was formed, the density is 92.6% of the theoretical density.

For the remaining samples, the evolution of the bulk density values with the treatment temperature is shown in **Figure 8**. In this case, we can see the same trend for this set of samples.
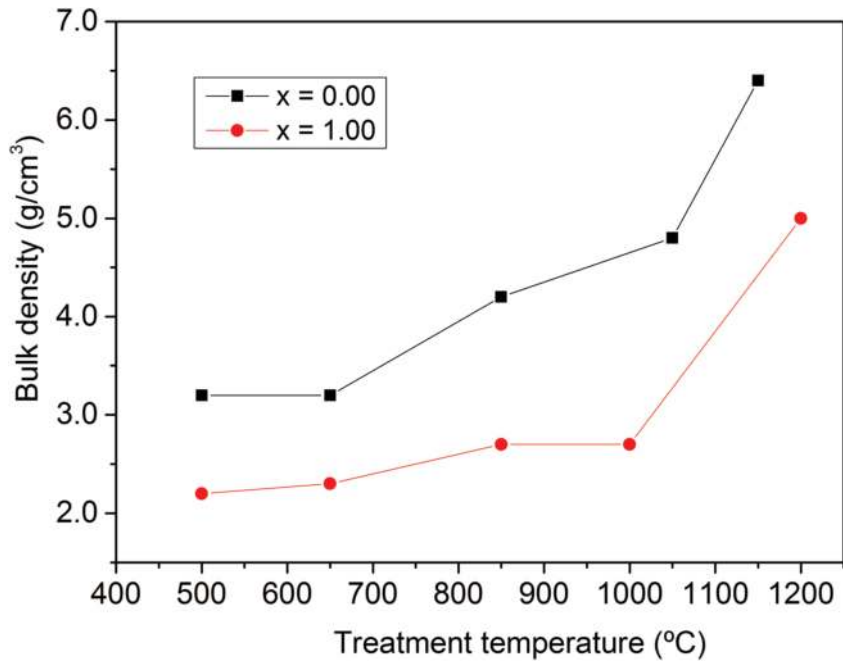
Figure 7. Bulk density of $(Bi_{1-x}Fe_x)NbO_4$ samples for $x = 0.00$ and $x = 1.00$.

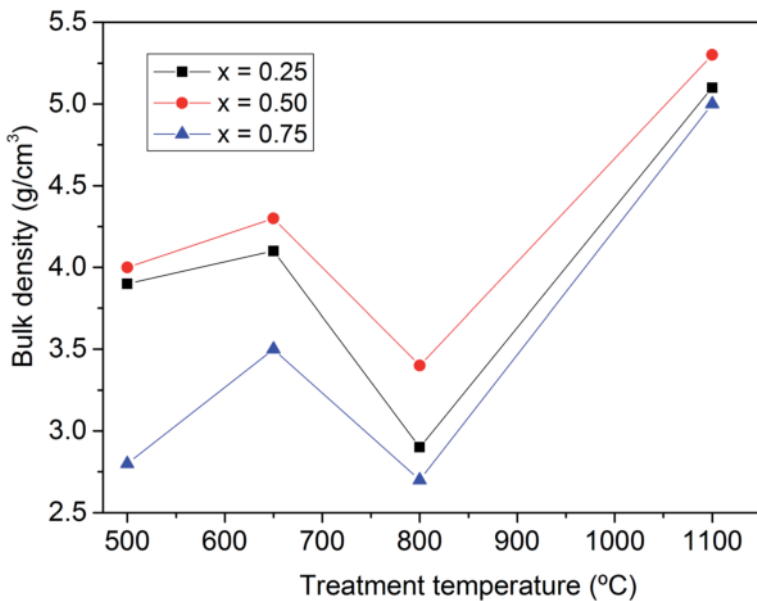**Figure 8.** Bulk density of $(Bi_{1-x}Fe_x)NbO_4$ samples for $x = 0.25$, $x = 0.50$, and $x = 0.75$.

The bulk density increases when the treatment temperature increases for 650°C, decreases for the treatment at 800°C, reaching a minimum value, and increases again with the higher treatment temperature. Regardless of the heat treatment, the samples with higher bulk density are the ones with $x = 0.50$.

2.3.5. Morphological characterization

In **Figure 9**, SEM micrographs of the samples with $x = 0.25$ and 0.50, treated at 650°C, are shown. In these samples, where the same phases were identified, we can see particles with spherical shape and diameter of 0.2 μm. Increasing the amount of iron, a decrease in porosity is detectable, a result that is coherent with the increase in density, previously analyzed.
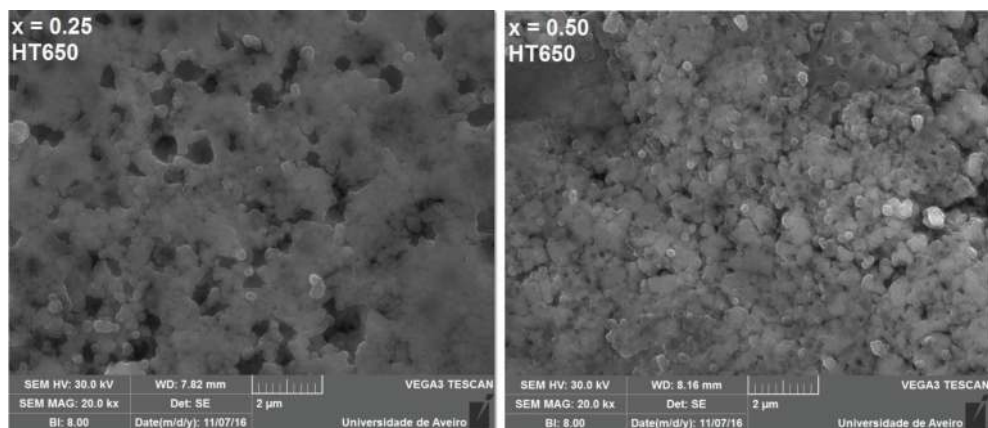

Figure 9. SEM micrographs of the samples with $x = 0.25$ and $x = 0.50$, treated at 650°C.

2.3.6. Microwave dielectric properties

In **Figure 10** is presented the transmission results obtained with the 2.7 GHz cavity, for the cases of the cavity only with the sample holder, with the sample holder filled with PTFE and filled with the samples with $0.25 \leq x \leq 0.75$, treated at 650°C. The expected shift in the resonant frequency of the cavity, Δf, is observed.

Since this shift, Δf, can be related to the real part of the complex permittivity, ε', it is expected that the sample with $x = 0.75$ presents the lowest ε', followed by the sample with $x = 0.25$ and finally the sample with $x = 0.50$, with the highest dielectric constant of this series of samples. This prediction will be confirmed later.

Figure 11 shows the real and the imaginary parts of the complex permittivity at 2.7 GHz, as function of the treatment temperatures, for the samples with $x = 0.00$ and $x = 1.00$.
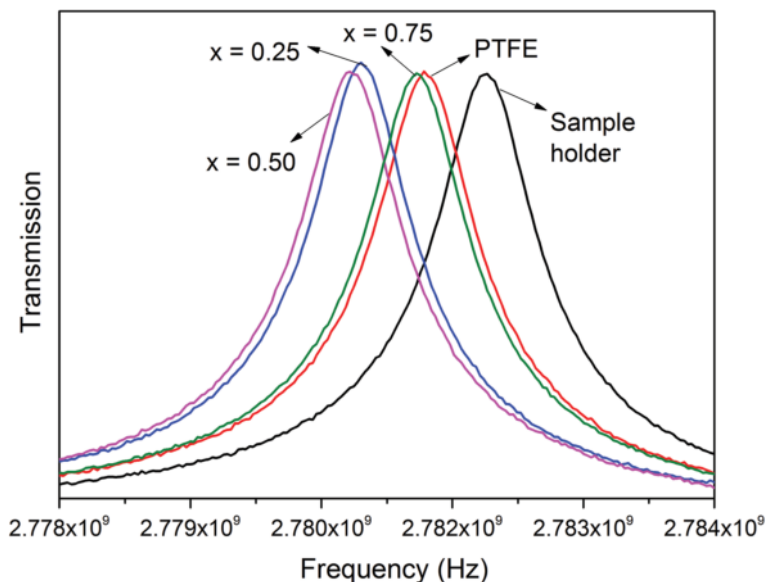
Figure 10. Transmission of the unperturbed and perturbed 2.7 GHz cavity, for $0.25 \leq x \leq 0.75$ $(Bi_{1-x}Fe_x)NbO_4$ samples, treated at 650°C.

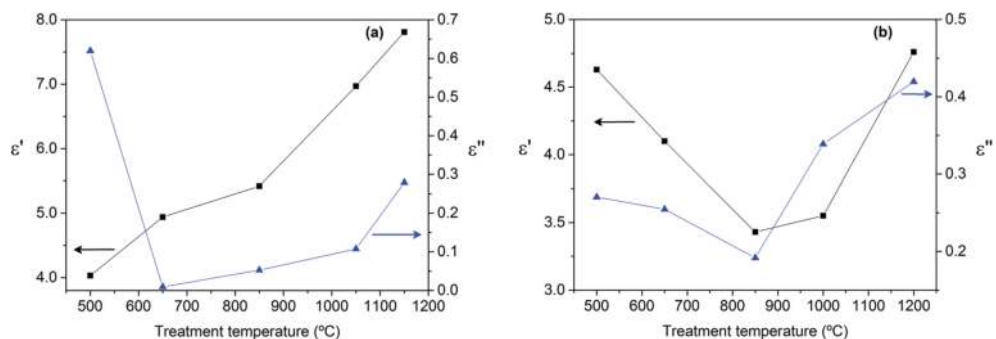**Figure 11.** Calculated ε' and ε'' of $(Bi_{1-x}Fe_x)NbO_4$ samples for (a) $x = 0.00$ and(b) $x = 1.00$, at room temperature.

For the samples with $x = 0.00$, **Figure 11(a)** shows that ε' values increase with the treatment temperature. The same trend was previously seen for the bulk density, suggesting that the dielectric constant increase with temperature is due to the density increase. With the exception of the sample treated at 500°C, where $BiNbO_4$ presence is still reduced, the dielectric losses also show the same evolution, increasing with the treatment temperature.

Figure 11(b) shows that for the samples with $x = 1.00$, the dielectric constant and the dielectric losses follow the same trend.

In **Figure 12**, it is presented the dielectric constant for the samples with $0.25 \leq x \leq 0.75$, as function of the treatment temperatures. Once more, the experimental data suggests that the increase of the bulk density is determinant for the increase of the dielectric constant. Nevertheless, the samples treated at 1100°C, besides the higher ε' values, also show the higher losses.

Table 3 resumes the calculated ε' and ε'' for the different samples.
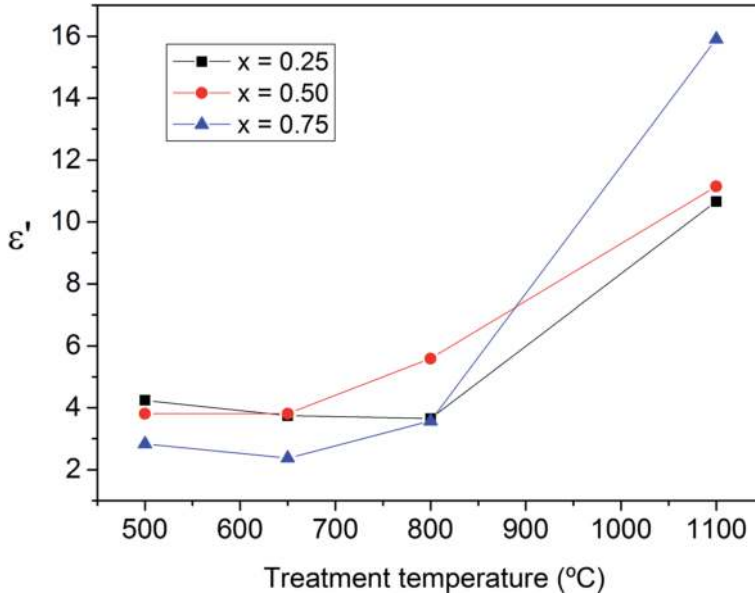
Figure 12. Calculated ε' for $0.25 \leq x \leq 0.75$ ($Bi_{1-x}Fe_x$)NbO_4 samples, at room temperature.

x		HT 500	HT 650	HT 800	HT 850	HT 1000	HT 1050	HT 1100	HT 1150	HT 1200
0.00	ε'	4.03	4.94	–	5.42	–	6.97	–	7.81	–
	ε''	0.62	0.01	–	0.05	–	0.11	–	0.28	–
0.25	ε'	4.24	3.74	3.65	–	–	–	10.66	–	–
	ε''	0.08	0.06	0.07	–	–	–	0.22	–	–
0.50	ε'	3.81	3.81	5.59	–	–	–	11.15	–	–
	ε''	0.09	0.09	0.15	–	–	–	0.35	–	–
0.75	ε'	2.83	2.37	3.57	–	–	–	15.91	–	–
	ε''	0.08	0.03	0.15	–	–	–	2.59	–	–
1.00	ε'	4.63	4.10	–	3.43	3.55	–	–	–	4.76
	ε''	0.27	0.25	–	0.19	0.34	–	–	–	0.42

Table 3. Calculated ε' and ε'' for different samples.

2.4. Conclusion

We can conclude that the $(Bi_{1-x}Fe_x)NbO_4$ ceramic powders were prepared successfully by the sol-gel method.

For $x = 0.00$, this method allows the formation of orthorhombic $BiNbO_4$ at lower temperatures than other preparation techniques. Both α and β phases can be stable in different temperature regions, below 850 and above 1050°C, respectively.

Furthermore, the density of the obtained samples was very promising, since no additives were used in the host samples.

The substitution of bismuth by iron was successful, since the two non-stoichiometric phases, $Bi_{1.34}Fe_{0.66}Nb_{1.34}O_{6.35}$ and $Bi_{1.721}Fe_{1.056}Nb_{1.134}O_7$, were obtained. Moreover, one can conclude that the inclusion of iron inhibits the formation of low- and high-temperature triclinic bismuth niobate.

Concerning the dielectric characterization, the small perturbation technique proved to be very practical for dielectric measurements on ceramic materials, featuring important advantages, as the easy sample preparation, the absence of measurement contacts, and the simplicity of the calculations.

The dielectric study revealed that, for $x = 0.00$, the dielectric constant increases with the increase of the sintering temperature, with the dielectric losses showing the same trend.

With the inclusion of iron, the highest ε' values were obtained for the highest treatment temperature; however, only the samples with $x = 0.25$ and 0.50 showed ε'' acceptable values.

Author details

Susana Devesa*, Manuel P.F. Graça and Luís C. Costa

*Address all correspondence to: susana_devesa@hotmail.com

I3N and Physics Department, University of Aveiro, Aveiro, Portugal

References

[1] Filho R.C., Araújo J.H., Ginani M.F., d'Assunção A.G., Martins R.A., d'Assunção A.G., Mendonça L.M. Simulation and measurement of inset-fed microstrip patch antennas on $BiNbO_4$ substrates. Microwave and Optical Technology Letters. 2010;**52**(5):1034–1036. DOI: 10.1002/mop.25098

[2] Sebastian M.T., Jantunen H. Low loss dielectric materials for LTCC applications: a review. International Materials Reviews. 2008;**53**(2):57–90. DOI: 10.1179/174328008X277524

[3]   Płońska M., Czekaj D. Studies of temperature and fabrication methods influence on structure and microstructure of BiNbO$_4$ microwave electroceramics. Archives of Metallurgy and Materials. 2011;**56**(4):1169–1175. DOI: 10.2478/v10172-011-0131-8

[4]   Kim E.S., Choi W. Effect of phase transition on the microwave dielectric properties of BiNbO$_4$. Journal of the European Ceramic Society. 2006;**26**(10–11):1761–1766. DOI: 10.1016/j.jeurceramsoc.2005.09.003

[5]   Liou Y.C., Tsai W.C., Chen H.M. Low-temperature synthesis of BiNbO$_4$ ceramics using reaction-sintering process. Ceramics International. 2009;**35**(6):2119–2122. DOI: 10.1016/j.ceramint.2008.11.030

[6]   Sales A.J.M., Oliveira P.W.S., Almeida J.S., Costa M.M., Rodrigues H.O., Sombra A.S.B. Copper concentration effect in the dielectric properties of BiNbO$_4$ for RF applications. Journal of Alloys and Compounds. 2012;**522**:264–270. DOI: 10.1016/j.jallcom.2012.07.025

[7]   Radha R., Gupta U.N., Samuel V., Muthurajan H., Kumar H.H., Ravi V. A co-precipitation technique to prepare BiNbO$_4$ powders. Ceramics International. 2008;**34**(6):1565–1567. DOI: 10.1016/j.ceramint.2007.03.022

[8]   Zhou D., Wang H., Yao X., Wei X., Xiang F., Pang L. Phase transformation in BiNbO$_4$ ceramics. Applied Physics Letters. 2007;**90**(17):2910. DOI: 10.1063/1.2732833

[9]   Zhai H.F., Qian X., Kong J.Z., Li A.D., Gong Y.P., Li H., et al. Abnormal phase transition in BiNbO$_4$ powders prepared by a citrate method. Journal of Alloys and Compounds. 2011;**509**(42):10230–10233. DOI: 10.1016/j.jallcom.2011.08.077

[10] Radha R., Muthurajan H., Rao N.K., Pradhan S., Gupta U.N., Jha R.K., Mirji S.A., et al. Low temperature synthesis and characterization of BiNbO$_4$ powders. Materials Characterization. 2008;**59**(8):1083–1087. DOI: 10.1016/j.matchar.2007.08.026

[11] Xu C., He D., Liu C., Wang H., Zhang L., Wang P., et al. High pressure and high temperature study the phase transitions of BiNbO$_4$. Solid State Communications. 2013;**156**:21–24. DOI: 10.1016/j.ssc.2012.11.007

[12] Kagata H., Inoue T., Kato J., Kameyama I. Low-fire bismuth-based dielectric ceramics for microwave use. Japanese Journal of Applied Physic. 1992;**31**:3152–3155. DOI:10.1143/JJAP.31.315

[13] Wang N., Zhao M.Y., Yin Z.W., Li W. Low-temperature synthesis of β-BiNbO$_4$ powder by citrate sol–gel method. Materials Letters. 2003;**57**(24–25):4009–4013. DOI: 10.1016/S0167-577X(03)00256-8

[14] Tzou W.C., Yang C.F., Chen Y.C., Cheng P.S. Improvements in the sintering and microwave properties of BiNbO$_4$ microwave ceramics by V$_2$O$_5$ addition. Journal of the European Ceramic Society. 2000;**20**(7):991–996. DOI: 10.1016/S0955-2219(99)00228-9

[15] Zhou D., Wang H., Yao X., Liu Y. Microwave dielectric properties of low-firing BiNbO$_4$ ceramics with V$_2$O$_5$ substitution. Journal of Electroceramics. 2008;**21**(1–4):469–472. DOI: 10.1007/s10832-007-9223-2

[16] Almeida J.S., Fernandes T.S.M., Sales A.J.M., Silva M.A.S., Júnior G.P., Rodrigues H.O., et al. Study of the structural and dielectric properties of Bi_2O_3 and PbO addition on $BiNbO_4$ ceramic matrix for RF applications. Journal of Materials Science: Materials in Electronics. 2011;**22**(8):978–987. DOI: 10.1007/s10854-010-0247-z

[17] Yang Y., Ding S., Yao X. Influences of Fe_2O_3 additives on the dielectric properties of $BiNbO_4$ ceramics under different sintering atmosphere. Ceramics International. 2004;**30**(7):1341–1345. DOI: 10.1016/j.ceramint.2003.12.110

[18] Devesa S., Graça M.P., Henry F., Costa L.C. Microwave dielectric properties of $(Bi_{1-x}Fe_x)NbO_4$ ceramics prepared by the sol–gel method. Ceramics International. 2015;**41**(6):8186–8190. DOI: 10.1016/j.ceramint.2015.03.038

[19] Butee S.P., Kambale K.R., Upadhyay S., Bashaiah S., Raju K.J., Panda H. Synthesis and microwave dielectric behavior of $(Bi_{1-x}Pb_x)NbO_4$ ceramics. Journal of Advanced Dielectrics. 2016;**6**(01):1650006. DOI: 10.1142/S2010135X16500065

[20] Shihua D., Xi Y., Yu M., Puling L. Microwave dielectric properties of $(Bi_{1-x}R_x)NbO_4$ ceramics (R= Ce, Nd, Dy, Er). Journal of the European Ceramic Society. 2006;**26**(10):2003–2005. DOI: 10.1016/j.jeurceramsoc.2005.09.049

[21] Wang N., Zhao M.Y., Yin Z.W., Li W. Effects of complex substitution of La and Nd for Bi on the microwave dielectric properties of $BiNbO_4$ ceramics. Materials Research Bulletin. 2004;**39**(3):439–448. DOI: 10.1016/j.materresbull.2003.10.016

[22] Tzou W.C., Yang C.F., Chen Y.C., Cheng P.S. Microwave dielectric characteristics of $(Bi_{1-x}Sm_x)NbO_4$ ceramics. Ceramics international. 2002;**28**(1):105–110. DOI: 10.1016/S0272-8842(01)00064-5

[23] Wang N., Zhao M.Y., Yin Z.W. Effects of Ta_2O_5 on microwave dielectric properties of $BiNbO_4$ ceramics. Materials Science and Engineering: B. 2003;**99**(1):238–242. DOI: 10.1016/S0921-5107(02)00464-6

[24] Butee S., Kulkarni A.R., Prakash O., Aiyar R.P.R.C., Sudheendran K., Raju K.J. Effect of lanthanide ion substitution on RF and microwave dielectric properties of $BiNbO_4$ ceramics. Journal of Alloys and Compounds. 2010;**492**(1):351–357. DOI: 10.1016/j.jallcom.2009.11.093

[25] Almeida C.G., Andrade H.M.C., Mascarenhas A.J.S., Silva L.A. Synthesis of nanosized β-$BiTaO_4$ by the polymeric precursor method. Materials Letters. 2010;**64**(9):1088–1090. DOI: 10.1016/j.matlet.2010.02.020

[26] Gaikwad A.B., Navale S.C., Samuel V., Murugan A.V., Ravi V. A co-precipitation technique to prepare $BiNbO_4$, $MgTiO_3$ and $Mg_4Ta_2O_9$ powder. Materials Research Bulletin. 2006;**41**(2):347–353. DOI:10.1016/j.materresbull.2005.08.01

[27] Maruyama Y., Izawa C., Watanabe T. Synthesis of by the flux method. ISRN Materials Science. 2012;**2012**:170362. DOI: 10.5402/2012/170362

[28] Shlyakhtin O.A., Orlov A.V., Oh Y.J. Liquid phase low temperature sintering of niobate and cerate fine powders. Journal of Electroceramics. 2006;**17**(2–4):405–413. DOI: 10.1007/s10832-006-9711-9

[29] Siqueira K.P., Moreira R.L., Dias A. Synthesis and crystal structure of lanthanide ortho-niobates studied by vibrational spectroscopy. Chemistry of Materials. Chemistry of Materials. 2010;**22**(8):2668–2674. DOI: 10.1021/cm100173p

[30] Henry F., Berteaud A.J. New measurement technique for the dielectric study of solutions and suspensions. Journal of Microwave Power. 1980;**15**(4):233–242.

[31] Henry F. Contribution a l'etude des processus d'hydratation [thesis]. France: Universite Pierre et Marie Curie; 1982.

[32] Costa L.C., Devesa S., André P., Henry F. Microwave dielectric properties of polybutylene terephtalate (PBT) with carbon black particles. Microwave and Optical Technology Letters. 2005;**46**(1):61–63. DOI: 10.1002/mop.20901

[33] Costa L.C., Henry F. The impact of blue inorganic pigments on the microwave electrical properties of polymer composites. International Journal of Microwave Science and Technology. 2012;**2012**:628237. DOI: 10.1155/2012/628237

[34] Devesa S., Graça M.P., Costa L.C. Structural, morphological and dielectric properties of $BiNbO_4$ ceramics prepared by the sol–gel method. Materials Research Bulletin. 2016;**78**:128–133. DOI: 10.1016/j.materresbull.2016.02.035

[35] Shim S.H., Duffy T.S. Raman spectroscopy of Fe_2O_3 to 62 GPa. American Mineralogist. 2002;**87**(2–3):318–326. DOI: 10.2138/am-2002-2-314

[36] Kumari T.S.D., Gandhi R.V., Rahul G., Kamalanathan G., Kumar T.P., Jeyakumar D., et al. Electrochemical lithium insertion behavior of $FeNbO_4$: Structural relations and in situ conversion into $FeNb_2O_6$ during carbon coating. Materials Chemistry and Physics. 2014;**145**(3):425–433. DOI: 10.1016/j.matchemphys.2014.02.031

[37] Cho I.S., Lee S., Noh J.H., Choi G.K., Jung H.S., Kim D.W., et al. Visible-light-induced photocatalytic activity in $FeNbO_4$ nanoparticles. The Journal of Physical Chemistry C. 2008;**112**(47):8393–18398. DOI: 10.1021/jp807006g

[38] Devesa S., Graça M.P., Henry F., Costa L.C. Dielectric properties of $FeNbO_4$ ceramics prepared by the sol–gel method. Solid State Sciences. 2016;**61**:44–50. DOI: 10.1016/j.solidstatesciences.2016.09.005

[39] Roth R.S., Waring J.L. Ixiolite + other polymorphic types of $FeNbO_4$. American Mineralogist. 1964;**49**(3–4):0003-004X.